CHEMISTRY OF MATERIALS

pubs.acs.org/cm Article

Effects of Hydrofluoric Acid Concentration on the Density of Silanol Groups and Water Adsorption in Hydrothermally Synthesized Transition-Metal-Substituted Silicalite-1

Daniel T. Bregante, David S. Potts, Ohsung Kwon, E. Zeynep Ayla, Jun Zhi Tan, and David W. Flaherty*

Cite This: https://dx.doi.org/10.1021/acs.chemmater.0c02405 Read Online

ACCESS | Metrics & More | Article Recommendations | Supporting Information

ABSTRACT: The type and density of structural defects within zeolites and zeotypes affect the stabilities of adsorbed species, which, in turn, impact the performance of these materials as catalysts and adsorbents. Despite the recognized importance of silanol groups (SiOH) on the properties of a zeolite catalyst or adsorbent, the densities of SiOH have not been quantitatively linked to the concentration of hydroxide (OH^-) and fluoride (F^-) ions within the synthesis gel. Here, we present a method for the synthesis of siliceous or heteroatom-substituted MFI zeolites (M-MFI; M = Si, Ti, Nb, or Ta) with tunable densities of SiOH, which depend simply on the ratio of hydrofluoric acid (HF) to structure-directing agent (SDA; tetrapropylammonium hydroxide) used within the synthesis gel. The equilibrated ion exchange between OH^- and F^- ions forms tetrapropylammonium fluoride *in situ*, which does not lead to the formation of SiOH defects within M-MFI. Comparisons of infrared spectra from 15 distinct M-MFI materials show that the densities of SiOH groups within M-MFI decrease linearly with the ratio of HF/SDA, independent of the identity of the heteroatom within the framework. Materials synthesized within purely OH^- media possess SiOH densities 3 and 100 times greater than analogous materials synthesized with HF/SDA ratios of 1 and 1.5, respectively. The use of HF forms metal fluoride complexes, detected by Raman spectroscopy, which are not readily incorporated into the zeolite framework during synthesis and lead to a decrease in the efficiency of transition-metal incorporation with increasing amounts of HF. The quantity of the heteroatom incorporated into the framework increases linearly with the concentration of metal precursor in the synthesis gel, which provides a method to mitigate the lower yields introduced by the use of HF. Comparisons between H_2O vapor adsorption isotherms show that M-MFI materials synthesized with an HF/SDA ratio of 1.5 adsorb 4−10-fold less H_2O than M-MFI synthesized with equal amounts of HF and SDA and 100 times less H_2O than M-MFI synthesized in OH^- media. Comparisons of water uptake within hydrophobic M-MFI materials show that framework Ti and Nb sites stabilize 5 and 7−8 H_2O molecules, respectively, near saturation vapor pressures. These findings provide a flexible strategy to control the densities of silanol and hydroxyl groups (e.g., Nb-OH) within MFI and will likely extend to the synthesis of other zeolite frameworks.

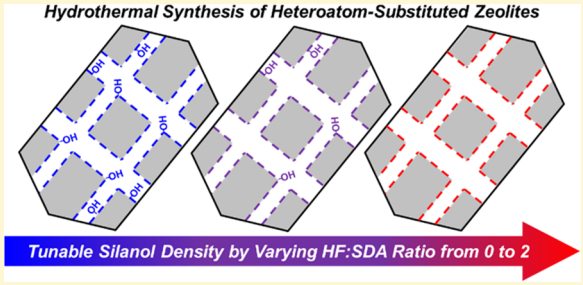

Downloaded via UNIV ILLINOIS URBANA-CHAMPAIGN on August 27, 2020 at 00:12:54 (UTC).
See https://pubs.acs.org/sharingguidelines for options on how to legitimately share published articles.

1. INTRODUCTION

The concept of differentiating molecules by their size and shape drives the development of zeolite and zeotype materials for catalysis and adsorption. The sub-nanometer sized pores of these materials can stabilize adsorbates or transition states through interactions between the guest molecules and the confining voids.[1−7] Van der Waals interactions among reactive species and pore walls provide the most significant differences in the free energies of adsorption and activation when pores are largely vacant.[1,4] Experiments[8−12] and simulations[13,14] show that both polar and nonpolar surface functions interact with reactive intermediates through outer-sphere interactions within solvent-filled pores (e.g., depending on solvent structure and reorganization), in ways that are distinct from dispersive interactions between surface intermediates and pore walls often invoked for gas-phase catalysis. Consequently, the controlled functionalization of micropores to control the composition and structure of solvent molecules near active sites is an attractive method to direct the chemical interactions among adsorbates, polar surfaces, and solvent structures.

The role of silanol density, commonly described as hydrophobic or hydrophilic effects, on catalysis and separations in zeolites has been an extensive area of research for decades.[11,15−21] For example, H^+-form Al-substituted silicalite-1 (H^+-Al-MFI) synthesized in OH^- media adsorbs 4 times as much H_2O as hydrophobic materials crystallized in F^- media.[18] The uptake of ethanol, however, does not change

Received: June 9, 2020
Revised: August 6, 2020
Published: August 10, 2020

© XXXX American Chemical Society

https://dx.doi.org/10.1021/acs.chemmater.0c02405
Chem. Mater. XXXX, XXX, XXX−XXX

with the density of SiOH within these materials, which suggests that specific hydrogen-bonding interactions among SiOH and H_2O molecules provide a basis to selectively separate components of aqueous solutions of ethanol.[18] In contrast, Tsapatsis and Siepmann have recently shown that siliceous silicalite-1 (Si-MFI) synthesized in OH^- media adsorbs 33% more ethanol than hydrophobic materials synthesized with an equimolar amount of ammonium fluoride (NH_4F) to tetrapropylammonium bromide.[22] Similarly, Si-MFI synthesized in OH^- media adsorbs 10−25 times more diol (1,2-butanediol, propylene diol, and ethylene glycol) than hydrophobic Si-MFI synthesized in F^- media, which was attributed to hydrogen-bonding interactions among silanol defects and the diol adsorbates.[23] The comparisons among these investigations suggest that polar functions (e.g., SiOH in Si-MFI, Brønsted acid sites in H^+-Al-MFI) within the MFI framework can form stabilizing hydrogen bonds with adsorbates, and the number and strength of these bonds depend upon the hydrogen bond donor−acceptor number of the adsorbate. These results also imply that the strengths of these interactions depend upon the density of SiOH within the zeolite pores.

Metal atoms substituted into zeolite frameworks can also stabilize specific solvent structures. For example, Bukowski et al. have recently used ab initio molecular dynamics to show that interactions between H_2O and Lewis acidic Sn atoms within BEA stabilize small H_2O clusters that comprise 5−6 H_2O molecules.[13] In comparison, H^+ sites within H^+-Al-MFI stabilize 8 H_2O molecules within liquid H_2O that has been identified as a hydronium cation surrounded by a seven-membered solvation shell.[24] As such, it is important to consider changes in solvent composition and structure that is due to heteroatoms within the framework, in addition to changes that result from nearby SiOH groups.

Interactions among SiOH functions, reactive species, metal active sites, and H_2O influence the rates and selectivities for methanol-to-hydrocarbons (MTH),[25,26] alkene epoxidations,[11,12,27−29] glucose isomerization,[8,9,17] alcohol dehydration,[24,30] and Baeyer−Villiger (BV)[31] oxidation reactions in heteroatom-substituted zeolites. For example, the initial conversion of methanol is noticeably greater within H^+-Al-MFI synthesized within F^- media than within OH^- media during MTH catalysis, purportedly because SiOH defects stabilize H_2O that form as a byproduct, which compete for active sites.[25] Moreover, H^+-Al-MFI synthesized in F^- media deactivates much more slowly than materials synthesized in OH^- media because SiOH defects stabilize aromatic precursors to coke.[25] In the context of alkene epoxidation, Ti-BEA that contain significant densities of SiOH defects stabilize H_2O clusters near active sites that must reorganize upon the formation of epoxidation transition states.[11,12] The reorganization of these solvent structures leads to large increases in the excess entropy of the transition states and results in rates of epoxidation that increase by a factor of 100 between hydrophobic Ti-BEA relative to materials that contain nearly 5 silanol nests per unit cell. Hydrophobic Ti- and Sn-BEA catalyze the aqueous-phase isomerization of glucose with rates that are 5−50 times greater than their hydrophilic analogues.[8,17,32,33] The presence of H_2O that is localized at or near Ti and Sn atoms within hydrophilic materials competes for active sites and forms hydrogen-bonded structures with glucose molecules that greatly decrease the entropy of the transition states.[34] Rates for BV oxidation of cyclohexanone with H_2O_2 are 5 times greater on hydrophilic Sn-BEA (synthesized through postsynthetic modification) than on hydrophobic Sn-BEA,[31] which was attributed to stabilizing interactions between the hydrophilic surfaces and the ketone reactant. In general, water and other protic molecules form intricate structures within zeolites through hydrogen bonds with the surrounding pore walls that impact the stability of adsorbates, intrapore diffusion coefficients, and surface reactions. Consequently, it is clear that the hydrophilic nature of a zeolite affects the catalytic performance of a material.

The silanol density of a given zeotype has traditionally been controlled through hydrothermal synthesis in either a hydroxide (OH^-) or a fluoride (F^-) media (Scheme 1).[18,35]

Scheme 1. Hydrothermal Synthesis of Zeolites in Hydroxide Media Leads to Hydrophilic Materials with Significant Densities of Silanol Groups, While Zeolites Crystallized in Fluoride Media Contain Fewer Silanol Defects and Are Hydrophobic in Comparison

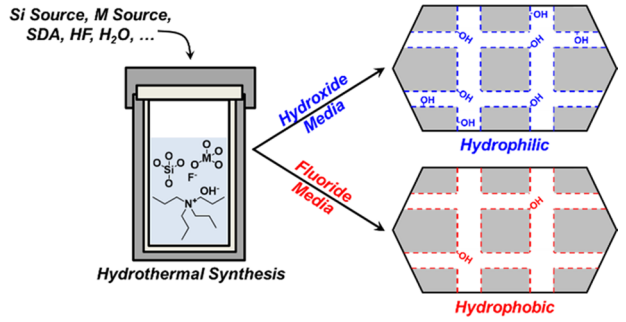

Hydrothermal synthesis involves the crystallization of a zeolite from a synthesis gel that contains a silicon source and a structure-directing agent (SDA; e.g., alkali,[36] tetraalkylammonium,[36−38] imidazolium,[37,39] diquaternaryammonium,[36−38,40] phosphonium,[37] or diquarternaryphosponium[38,40] cations). The presence of OH^- anions leads to the formation of anionic framework vacancy defects because solvated OH^- requires that zeolite precursor units self-assemble around these ions. In contrast, F^- ions form a tighter ion pair with the cationic SDA and yield materials with lower densities of internal silanol defects.[41,42] The majority of studies on hydrophilic and hydrophobic zeolites compare materials synthesized with SDAs that are predominantly in OH^- form or that are combined with an equimolar amount of a F^- source (e.g., hydrofluoric acid (HF) or NH_4F).[16,22,23,41,43,44] The functional dependence of the final SiOH density on the concentration of F^- ions within the synthesis gel has, however, not been determined. Moreover, the literature shows that the presence of F^- generally decreases the efficiency of heteroatom incorporation into synthesized materials,[9,19,45,46] which affects the density of active sites within the final zeolite. Consequently, the community would greatly benefit from synthetic methods and characterization data that demonstrate how the concentration of F^- ions affects the incorporation of heteroatoms and can be used to control SiOH density within a given zeolite.

Here, we report the hydrothermal synthesis of siliceous and heteroatom-incorporated MFI zeolites (M-MFI, where M represents Si, Ti, Nb, and Ta) with control over the density of SiOH functions. MFI materials are synthesized using tetrapropylammonium hydroxide (TPAOH) and varying

https://dx.doi.org/10.1021/acs.chemmater.0c02405
Chem. Mater. XXXX, XXX, XXX−XXX

amounts of HF (HF/TPAOH ratios from 0 to 2) to control the density of SiOH groups. Transmission infrared spectra of dehydrated materials show that the relative density of SiOH functions decreases by ∼66% when the HF/SDA ratio increases from 0 to 1. M-MFI with nearly undetectable SiOH densities form when the HF-to-SDA ratio meets or exceeds a value of 1.5. Ion exchange between HF and TPAOH forms TPAF *in situ* by a reversible reaction, presumably near equilibrium. Therefore, the near-complete ion exchange requires a stoichiometric excess of HF. F^- ions, however, ligand-exchange with transition-metal complexes to form $M(OH)_xF_y$ species that are detected by Raman spectroscopy. These metal fluoride complexes do not incorporate effectively into the MFI framework. Consequently, the use of excess HF produces materials with significantly fewer SiOH functions but also decreases the efficiency with which the heteroatoms incorporate into the framework.

Vapor-phase H_2O adsorption isotherms show functional differences in M-MFI materials that arise from differences in the density of SiOH. H_2O adsorption resembles a type I isotherm for all materials; yet, the amount of H_2O adsorbed increases monotonically with the density of SiOH groups. Hydrophobic M-MFI synthesized using HF-to-SDA ratios equal to 1.5 adsorb ∼10- and ∼100-fold less H_2O than M-MFI synthesized with HF-to-SDA ratios of 1 and 0, respectively. M-MFI synthesized using HF-to-SDA ratios less than unity adsorb indistinguishable amounts of H_2O because SiOH groups spontaneously nucleate H_2O clusters in these materials. Comparisons among hydrophobic M-MFI materials reveal that H_2O clusters preferentially adsorb to Lewis and Brønsted acid sites associated with the framework heteroatoms. Thermodynamic analysis of H_2O adsorption isotherms shows that Lewis acidic Ti atoms stabilize ∼5 H_2O, while Brønsted acidic Nb and Ta adsorption sites form structures consisting of 7−8 H_2O molecules within aqueous media, which may have implications for catalysis or separations. Collectively, the synthesis procedure presented here provides a simple and robust method that extends to the synthesis of other frameworks, which enables precise control over the density of SiOH groups within a zeolite material.

2. MATERIALS AND METHODS

2.1. Synthesis of Metal-Substituted Silicalite-1 (M-MFI). Titanium butoxide (TiBO; Sigma-Aldrich, 97%, reagent grade), niobium ethoxide (NbEO; Sigma-Aldrich, 99.95%, trace metal basis), tantalum ethoxide (TaEO; Sigma-Aldrich, 99.98%, trace metal basis), tetraethylorthosilicate (TEOS, Sigma-Aldrich, 98%, reagent grade), tetrapropylammonium hydroxide (TPAOH; Sachem, 40% in H_2O), hydrofluoric acid (HF; Sigma-Aldrich, 48−50% in H_2O), and H_2O (18.2 MΩ·cm) were used as received.

Metal-substituted MFI (M-MFI; M = Si, Ti, Nb, or Ta) was synthesized hydrothermally in either hydroxide or fluoride media. A desired amount of the metal precursor (i.e., TiBO, NbEO, or TaEO; see above) was dissolved in 27.7 g of TEOS in a polypropylene bottle with a screw cap to form a homogeneous solution that was subsequently cooled to 273 K. Separately, a mixture of 28.7 g of TPAOH and 50.5 g of H_2O was cooled to 273 K and was added slowly (over a period of ∼1 min) to the TEOS solution, which yielded a biphasic mixture. This solution was warmed to 298 K and stirred for 12 h to produce a clear homogeneous solution, which indicates successful hydrolysis of the metal precursor and TEOS. Solutions that are cloudy contain metal oxide nanoparticles that preclude the incorporation of the metal into the zeolite framework. In these cases, the solution was discarded and the synthesis was initiated with fresh reagents. The cover was then removed to completely evaporate the alcohol (e.g., ethanol, butanol) formed through hydrolysis of TEOS and the metal alkoxides. To ensure the complete evaporation of the alcohols, an additional 15 wt % of the calculated mass of the alcohols was evaporated over the course of 24−48 h and deionized H_2O was added to make up for the excess liquid evaporated. This solution was then loaded into a Teflon-lined stainless steel autoclave (Parr instruments, 125 cm^3). While in the Teflon liner, the desired amount of HF (warning: HF is extremely dangerous and should be handled very carefully) was added to the synthesis gel and stirred manually with a polypropylene spatula for ∼10 s prior to gelation. Notably, the addition of at least an equimolar amount of HF, with respect to TPAOH, increases the viscosity of the synthesis gel significantly. These steps yield a gel with the approximate composition of 1 Si: *a* M: 0.43 TPAOH: *b* HF: 28.3 H_2O, where *a* and *b* depend on the amount of metal precursor and HF used, respectively. A small amount of Ti- or Si-MFI seeds (5% by mass relative to SiO_2) from a previous synthesis in OH^- media was added to promote the crystallization of MFI. These autoclaves were then heated to 443 K while rotating (30 rpm) in a convection oven (Yamato, DKN602C) for a desired amount of time (72−792 h; see Section 3.1). The resulting solids were recovered by centrifugation, washed with H_2O, and dried for 16 h at 373 K. The dried solids were then heated in flowing air (100 cm^3 min^{-1}; Airgas, Ultra-zero grade) to 823 K at 1 K min^{-1} and held for 10 h to produce M-MFI materials that were bleached white in appearance. Typical zeolite yields were between 75 and 95%, by mass of SiO_2. Infrequently, the recovered solids appear off-white or yellow-brown; however, subsequent oxidative treatment in flowing air removes the residual organics likely responsible for these colors.

2.2. Characterization of M-MFI. The metal contents of all M-MFI were determined using energy-dispersive X-ray fluorescence (EDXRF). Finely ground M-MFI samples were loaded into a polypropylene sample holder (2.54 cm aperture), which was sealed with an ultralene film. These samples were loaded into a spectrometer (Shimadzu, EDX-7000) whose sample chamber was purged with He (Airgas, Ultra-zero grade) prior to measurement. Spectra were obtained between 0 and 30 keV (100 scans), and the relative intensities of the element-specific fluorescence features and their associated calibration factors were used to determine the percent, by mass, of each element within the sample.

The crystallinity of the MFI framework was measured through X-ray diffraction (XRD). The samples were loaded onto a polypropylene holder, and diffractograms were collected on an X-ray diffractometer (Bruker, D8) with Cu Kα radiation (0.15418 nm) under ambient conditions.

The presence of highly disperse M atoms (and absence of bulk or oligomeric MO_x domains) for M-MFI samples was inferred by the band edge energies, which were measured using diffuse reflectance UV−vis spectroscopy. Total reflectance spectra were measured under ambient conditions using a diffuse reflectance accessory (Harrick, Cricket) with a UV−vis−NIR spectrophotometer (Agilent, CARY 5). Prior to measurement, the samples were intimately mixed with magnesium oxide (MgO; Sigma-Aldrich, 99.995%) in a 1:10 ratio by mass.

The morphology of M-MFI samples was characterized using scanning electron microscopy (SEM). The samples were intimately ground and dispersed on a double-sided carbon tape, which was attached to an SEM holder. The samples were coated with a Au−Pd alloy using a sputter coater (Emitech, K575) to inhibit surface charging. This metal sample holder was loaded onto a microscope (JEOL, 6060) and was degassed prior to imaging. Micrographs were obtained using an accelerating voltage of 10 kV and a working distance of 10 mm.

The incorporation of heteroatoms into the MFI framework was inferred using attenuated total reflectance-infrared spectroscopy. The samples were pressed onto a diamond internal reflection element of an infrared spectrometer (Bruker, Alpha), and spectra (8 scans, 2 cm^{-1} resolution) were recorded at ambient conditions.

^{19}F nuclear magnetic resonance (NMR) spectra were collected on the supernatant from Si- and Ti-MFI-F(1.5) syntheses to detect the formation of Ti−F complexes. ^{19}F NMR spectra were collected on a

https://dx.doi.org/10.1021/acs.chemmater.0c02405
Chem. Mater. XXXX, XXX, XXX−XXX

Table 1. Molar Ratios of HF to TPAOH, Synthesis Times, Metal Loadings,[a] BET Surface Areas,[b] Micropore Volumes,[c] External Surface Areas,[c] Band Edge Energies,[d] and Relative Density of SiOH (ϕ_{IR})[e] within M-MFI-F(x)[f]

sample name	HF/TPAOH ratio	synthesis time (days)	metal loading (wt %)[a]	BET surface area (m^2 g^{-1})[b]	micropore volume (cm^3 g^{-1})[c]	external surface area (m^2 g^{-1})[c]	band edge energy (eV)[d]	ϕ_{IR}[e]
Si-MFI-F(0)	0	3	--	631	0.14	128	--	3.87
Si-MFI-F(0.33)	0.33	7	--	402	0.14	110	--	2.70
Si-MFI-F(0.66)	0.66	7	--	455	0.13	174	--	1.17
Si-MFI-F(1)	1	7	--	551	0.15	330	--	0.41
Si-MFI-F(1.25)	1.25	7	--	546	0.14	338	--	0.21
Si-MFI-F(1.5)	1.5	7	--	552	0.13	402	--	0.08
Ti-MFI-F(0)	0	3	0.27	399	0.15	126	4.8	3.31
Ti-MFI-F(0.33)	0.33	7	0.23	361	0.14	108	5.0	2.11
Ti-MFI-F(0.66)	0.66	7	0.22	364	0.14	304	5.0	2.05
Ti-MFI-F(1)	1	7	0.10	367	0.13	342	4.8	1.26
Ti-MFI-F(1.25)	1.25	7	0.06	443	0.14	398	4.8	0.25
Ti-MFI-F(1.5)	1.5	7	0.04	406	0.13	376	4.8	0.03
Nb-MFI-F(0)	0	5	0.57	444	0.15	122	4.8	3.04
Nb-MFI-F(1)	1	14	0.44	333	0.14	200	4.5	0.40
Nb-MFI-F(1.5)	1.5	14	0.31	368	0.14	320	4.6	0.10
Ta-MFI-F(0)	0	7	1.08	518	0.15	113	4.8	2.90
Ta-MFI-F(1)[e]	1	33	0.56	447	0.12	189	4.9	0.40
Ta-MFI-F(1.5)[e]	1.5	33	0.51	404	0.13	289	5.0	0.13

[a]Measured using EDXRF. [b]Determined from N_2 physisorption. [c]Calculated using the t-plot from N_2 physisorption. [d]Measured using DRUV−vis. [e]Quantified by infrared spectroscopy of dehydrated M-MFI-F(x). [f]The intended weight loadings of all Ti-, Nb-, and Ta-MFI-F(x) within Table 1 were 0.3, 0.6, and 1.2 wt %, respectively.

spectrometer (Varian, 600 NB) operating at 564 MHz. All spectra were referenced to $CFCl_3$ (1% $CFCl_3$ in $CDCl_3$), which has a ^{19}F chemical shift of 0 ppm.

Infrared (IR) spectra of dehydrated M-MFI were used to quantify the relative density of silanol groups within this series of materials. Vibrational spectra were obtained using a custom-built temperature-controlled transmission cell coupled to a Fourier-transform IR spectrometer (Bruker, Vertex 70) with a liquid N_2-cooled HgCdTe detector. Self-supporting catalyst wafers (~45 mg) were loaded into the transmission cell, which was configured with CaF_2 windows and connected to a gas manifold. All materials were first heated to 573 K at 10 K min^{-1} and held for >2 h in flowing He (50 cm^3 min^{-1}) to desorb water and volatile compounds. IR spectra (128 scans, 1 cm^{-1}) of the dehydrated M-MFI were then recorded at 573 K, and the corresponding background spectra were obtained with the empty cell at identical conditions.

Raman spectra of the supernatant recovered after the hydrothermal synthesis of Ti- and Si-MFI-F(1.5) samples, where 1.5 represents the HF-to-TPAOH ratio, were used to detect the formation of soluble titanium fluoride complexes that resist incorporation into the zeolite framework during hydrothermal synthesis. The supernatant from these syntheses was recovered by centrifugation. A portion of this liquid (20 cm^3) was dried at 353 K under flowing air (100 cm^3 min^{-1}) for 10 h to yield a thick gel. These gels were spread on glass microscope slides (VWR), and Raman spectra were collected on a spectrometer (Renishaw, inVia) equipped with a 532 nm laser. Spectra were obtained with line-scan mode using a long 50× objective such that the power density was approximately 0.4 mW μm^{-2}.

Gas-phase adsorption isotherms were collected on a volumetric adsorption instrument (Micromeritics, 3Flex). M-MFI samples were pelletized and sieved to retain particles greater than 180 μm in diameter. These samples were degassed by heating under vacuum (<7 × 10^{-4} Pa, 673 K) for 6 h prior to adsorption measurements. Vapor-phase H_2O adsorption measurements were conducted at room temperature (293 ± 1 K), while N_2 adsorption was conducted at 77 K. The H_2O used was degassed via one freeze−pump−thaw cycle prior to measurements.

3. RESULTS AND DISCUSSION

3.1. Tuning Silanol Density by Controlling the HF-to-SDA Ratio in the Synthesis Gel. Hydrothermal synthesis of transition-metal-substituted MFI (M-MFI; Si, Ti, Nb, or Ta) in hydroxide (OH^-) media, fluoride (F^-) media, or mixtures thereof produces materials with varying silanol (SiOH) densities. Each M-MFI sample is denoted as M-MFI-F(x), where x is the ratio of HF to TPAOH in the synthesis gel. All M-MFI-F(x) show X-ray diffraction patterns that are consistent with phase-pure MFI (Figure S1). The diffraction peaks that correspond to the (101) and (200) reflections[47] of Si-MFI at ~8 and ~9° decrease monotonically as the HF/TPAOH ratio decreases and span a range of 0.2° between HF/TPAOH ratios of 1.5 and 0 (Figure S2), suggesting that there is an expansion of the MFI framework. This is notably different from the contraction of the BEA framework due to the presence of $(SiOH)_x$ defects.[48,49] Interestingly, within Ti-, Nb-, and Ta-MFI samples, there does not appear to be a systematic change in the position of the (101) or (200) reflections. In all cases, M-MFI-F(x) possess the high Brunauer−Emmett−Teller (BET) surface areas and micropore volumes (0.12−0.15 cm^3 g^{-1}) characteristic of the MFI framework.[50,51] External surface areas (Table 1) increase with the HF/TPAOH ratio, which correlates with the concomitant increase in the average crystal size of the M-MFI materials (see below).

The time required to crystallize M-MFI-F(x) samples varies from 3 to more than 33 days and depends on the concentration of F^- ions and the identity of the heteroatom. The addition of HF into the synthesis gel increases the crystallization time considerably (Table 1; e.g., 3−7 days for Ti- and Si-MFI-F(0) versus M-MFI-F(1)). Zeolite precursors form from the condensation of anionic silyloxy species (e.g., $[SiO_2(OH)_2]^{2-}$, $[SiO(OH)_3]^-$) present in an acid−base equilibrium with $Si(OH)_4$ species.[52] The addition of HF lowers the pH of the synthesis gel, which consequently lowers

https://dx.doi.org/10.1021/acs.chemmater.0c02405
Chem. Mater. XXXX, XXX, XXX−XXX

the concentration of these anionic silyloxy species and slows the formation rates of the silicalite-1 precursors.[53]

The identity of the heteroatom incorporated into M-MFI-F(x) also affects rates of crystallization. For example, Si-, Ti-, Nb-, and Ta-MFI-F(0) require up to 3, 3, 5, or 7 days, respectively, under dynamic conditions to fully crystallize. These results agree with prior reports on how the time required to crystallize framework-substituted BEA changes depending on the identity of the heteroatom (e.g., Ti, Nb, Ta, Sn; see Section S6).[16,54,55] The differences in crystallization rates are exacerbated by the presence of F^- ions: Ta-MFI-F(x) requires up to 33 days to yield crystalline materials, while Si- and Ti-MFI-F(x) require only 7 days. It should be noted that the times reported for crystallization are not necessarily optimized. In our hands, Ta-MFI-F(1, 1.5) crystallized for 21 days contain large amorphous domains, detected by XRD; yet, they are phase-pure after 33 days under hydrothermal conditions (Figure S1).

Figure 1 shows representative scanning electron micrographs of Ti-MFI-F(0) and Ti-MFI-F(1). Ti-MFI synthesized in OH^- media consist of ~300 nm wide cuboids. The addition of F^- ions significantly increases the characteristic length of the MFI crystallites and forms plate-like structures that are 300−800 nm thick and 3−5 μm in length.

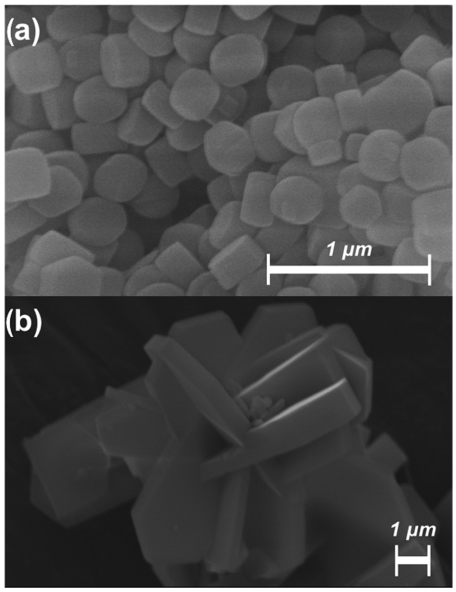

Figure 1. Scanning electron micrographs of (a) Ti-MFI-F(0) and (b) Ti-MFI-F(1).

The incorporation of metal atoms into the MFI framework can be confirmed by a combination of infrared (IR), Raman, and UV−vis spectroscopies. Figure 2 shows attenuate total reflectance-infrared spectra of M-MFI-F(0) samples containing several vibrational features between 800 and 1300 cm^{-1}. IR spectra of the analogous M-MFI-F(1.5) materials are shown in Figure S5. The strong features at 800, 1080, and 1230 cm^{-1} correspond to vibrational modes that are characteristic of zeolite frameworks.[56] The additional feature at 960 cm^{-1} within Ti-, Nb-, and Ta-MFI-F(0) and Ti-MFI-F(1.5) materials (Figures 2 and S5) corresponds to ν(Si−O−M) of framework-substituted heteroatoms.[56] All M-MFI-F(x) possess a single prominent UV−vis absorbance feature around 5.2−5.5 eV (Figure S3) that corresponds to the charge transfer from the 2p orbitals of oxygen to the 3d, 4d, or 5d orbitals of Ti^{4+}, Nb^{5+}, or Ta^{5+}, respectively.[11,49,57−59] The band gaps for these electronic transitions within M-MFI-F(x) materials are between 4.5 and 5.0 eV in all cases (Table 1) and are significantly greater than the band gaps reported for the analogous bulk metal oxides (i.e., 3.2 eV for TiO_2,[58] 3.4 eV for Nb_2O_5,[60] 3.9 eV for Ta_2O_5).[61] Finally, Figure S6 shows that the Raman spectra of all M-MFI-F(0) and M-MFI-F(1.5) contain only scattering features that are attributed to the MFI framework and do not possess any vibrational features that resemble bulk metal oxide domains (Section S5). Consequently, this combination of IR, UV−vis, and Raman spectroscopic evidence strongly suggests that the M atoms within each of these materials are highly disperse, incorporated into the MFI framework, and that M-MFI-F(x) samples possess few, if any, MO_x oligomers or larger agglomerates.

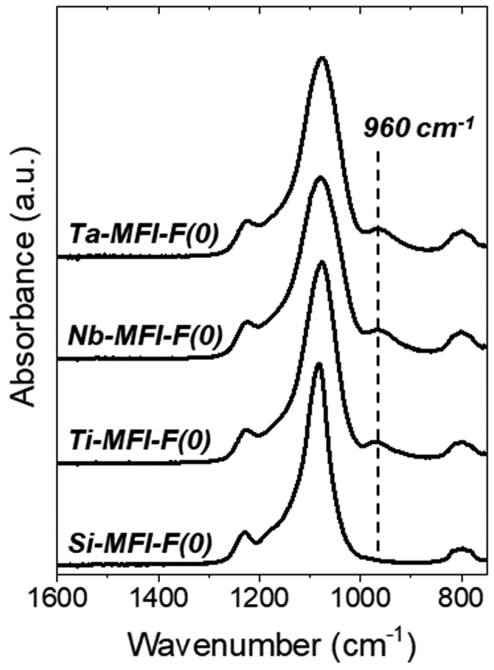

Figure 2. Infrared spectra of Si-, Ti-, Nb-, and Ta-MFI-F(0) at ambient conditions. All spectra are normalized to the framework vibration at ~1080 cm^{-1} and are vertically offset for clarity.

Infrared spectra of M-MFI-F(x) contain vibrational features that can be used as a quantitative estimate for the density of SiOH within a given material. Figure 3 shows a series of infrared (IR) spectra of Ti-MFI-F(x) (x = 0, 0.33, 0.66, 1, 1.25, and 1.5) at 573 K to desorb volatile compounds. IR spectra of the other M-MFI-F(x) materials are available in Figure S7. These spectra possess vibrational features at 1990 and 1865 cm^{-1} that correspond to ν(Si−O−Si) overtones from the MFI framework, while the broad features between 3300 and 3750 cm^{-1} are attributed to ν(O−H) of the SiOH within these materials.[31,62] The sharp feature at 3740 cm^{-1} corresponds to ν(O−H) of isolated SiOH, which do not interact with other SiOH species. The broad bimodal feature with peak centers at 3680 and 3540 cm^{-1} represents $(SiOH)_x$ groups that contain multiple, proximate hydrogen-bonded −OH functions.[11,63,64] M-MFI synthesized with HF/TPAOH ratios less than unity possess a broad vibrational feature around 3540 cm^{-1}, which likely corresponds to multiple $(SiOH)_x$ defects that interact through hydrogen-bonding interactions. When the HF/TPAOH ratios within the synthesis gel are greater than one,

https://dx.doi.org/10.1021/acs.chemmater.0c02405
Chem. Mater. XXXX, XXX, XXX−XXX

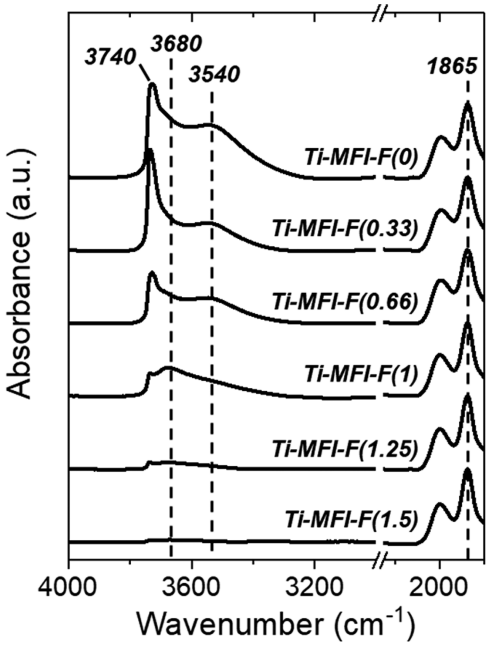

Figure 3. Infrared spectra of dehydrated Ti-MFI-F(x) (x = 0, 0.33, 0.66, 1, 1.25, 1.5) at 573 K (50 cm^{-3} min^{-1} He). All spectra are normalized to the ν(Si−O−Si) overtone at 1865 cm^{-1} and are vertically offset for clarity.

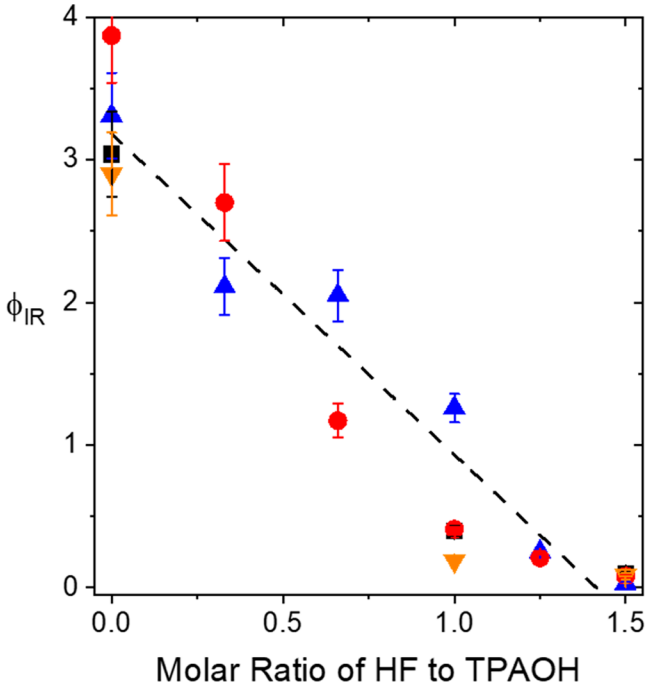

Figure 4. Relative SiOH densities, ϕ_{IR}, as a function of the HF/TPAOH molar ratio (i.e., x) for Si-MFI-F(x) (red ●), Ti-MFI-F(x) (blue ▲), Nb-MFI-F(x) (black ■), and Ta-MFI-F(x) (orange ▼). The dashed line represents a concatenated linear on all MFI materials.

the broad feature at 3540 cm^{-1} is greatly attenuated, which suggests that the ν(O−H) feature located at 3680 cm^{-1} reflects singular, noninteracting $(SiOH)_x$ defects. Unfortunately, the quantification of these densities (in units of (mol SiOH) (g^{-1})) requires spectral deconvolution of the broad ν(O−H) modes and extinction coefficients for each type of SiOH, which are not available.

Zeolites are crystalline forms of SiO_2 that contain predominantly Si−O−Si linkages. As such, ν(Si−O−Si) overtone stretches provide a convenient point of normalization for each IR spectra, to avoid irregularities in the pellets and circumvent the absence of extinction molar extinction coefficients for the different types of SiOH functions. A quantitative measure for the density of SiOH in M-MFI-F(x), defined as ϕ_{IR}, is thus determined by normalizing the area of ν(O−H) ($A_{\nu(O-H)}$) relative to that of the ν(Si−O−Si) overtone stretch at 1865 cm^{-1} ($A_{\nu(Si-O-Si)}$)

$$\phi_{IR} = \frac{A_{\nu(O-H)}}{A_{\nu(Si-O-Si)}} \quad (1)$$

Here, values of ϕ_{IR} represent the relative density of $(SiOH)_x$ among the M-MFI samples and do not correspond to the fraction of Si atoms that exist as SiOH. Figure 4 shows that values of ϕ_{IR} decrease linearly with the ratio of HF/TPAOH in the synthesis gel for Si-, Ti-, and Nb-MFI-F(x). When the molar ratio of HF/TPAOH in the synthesis gel increases from 0 to 1, the density of SiOH groups decreases by a factor of 4−8. An HF/TPAOH ratio of 1.5 leads to a 30−100-fold decrease in ϕ_{IR} in comparison to M-MFI-F(0). Further increases in the HF/TPAOH ratio, however, do not lead to additional changes in ϕ_{IR}. For example, Ti-MFI-F(2) (i.e., synthesized with an HF/TPAOH ratio of 2) possess a ϕ_{IR} value of 0.03, which is indistinguishable from Ti-MFI-F(1.5). The role of F^- ions reflects a complex network of chemical equilibria that depend on the concentration and identity of the ionic species (Section 3.2). Collectively, these findings show that the density of SiOH functions within M-MFI zeolites can be systematically varied by changing the HF-to-TPAOH ratio within the synthesis gel.

3.2. Ion-Exchange Reactions with Fluoride Anions That Affect Silanol Density and Metal Incorporation. Hydroxide anions lead to the formation of $(SiOH)_x$ defects because solvated OH^- requires that zeolite precursor units self-assemble around these ions. Fluoride ion exchanges with OH^-, which forms tighter ion pairs with the cationic SDAs and leads to materials with lower densities of internal silanol defects.[41,42] Common SDAs include cationic species (e.g., alkali,[36] tetraalkylammonium,[36−38] imidazolium,[37,39] diquaternaryammonium,[36−38,40] phosphonium,[37] and diquarternaryphosphonium;[38,40] Scheme 2) that are charge-balanced by a OH^- anion. Most studies that focus on the synthesis of hydrophobic materials use either fluoride-form SDAs or an equimolar amount of HF (to the OH^- form salt), which are equivalent when dissolved into an aqueous solution. Figures 3 and 4 and Table 1 show, however, that M-MFI-F(1) materials contain a smaller but still significant density of SiOH groups as an HF-to-TPAOH ratio of one decreases the density of SiOH functions by 4−8-fold. Greater quantities of HF (e.g., HF/TPAOH ratios equal to 1.5) further decrease the SiOH density to a value 30−100 times less than observed on samples synthesized in OH^- media. Materials created with these stoichiometric excesses of HF (i.e., $x \geq 1.5$) possess nearly undetectable densities of SiOH moieties.

TPAOH ion exchanges with HF to form TPAF in situ; however, the ion exchange is reversible and the concentrations of the species are dictated by equilibrium. The addition of excess HF to the synthesis gel biases the equilibrium between tetrapropylammonium hydroxide and tetrapropylammonium fluoride (Scheme 2) toward the products, which leads to fewer SiOH defects formed during hydrothermal synthesis. In the

https://dx.doi.org/10.1021/acs.chemmater.0c02405
Chem. Mater. XXXX, XXX, XXX−XXX

Scheme 2. Examples of Ion Exchange between Various Common Classes of Structure-Directing Agents in Hydroxide Form with HF to Form the Fluoride-Form SDA In Situ

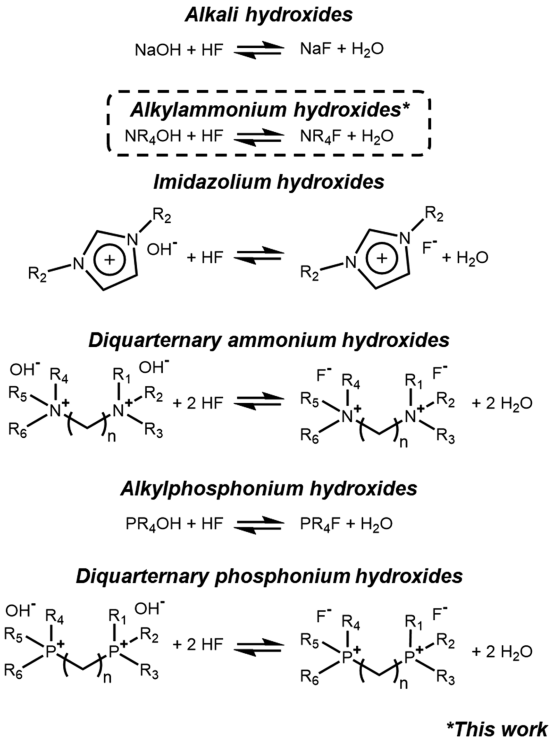

majority of studies on zeolite synthesis in fluoride media, hydrophobic materials are crystallized in synthesis gels that contain stoichiometric amounts of F^- and SDA. As such, this concept likely extends to other SDAs capable of ion exchange (see Scheme 2 for several examples), such that the HF/SDA ratio within the synthesis gel can be used to control the SiOH density for a variety of zeolite frameworks (e.g., CHA,[65,66] MFI,[18,22,67] BEA,[9,45,54] MWW,[68] CIT-5[69]) that are synthesized hydrothermally using cationic SDAs. While the use of HF to form SDA-F complexes in situ is expected to be extended to a variety of SDAs, the equilibrium that describes SDA-F formation likely depends on the chemical properties (e.g., pK_a) of the SDA, the pH of the synthesis gel, and the crystallization temperature.

The extent of heteroatom incorporation into the MFI framework depends on the concentration of F^- ions within the synthesis solution. The synthesis gels for the Ti-, Nb-, and Ta-MFI-F(x) materials described in Table 1 contained amounts of the heteroatom precursor intended to yield materials with transition-metal weight percentages of 0.3, 0.6, and 1.2, respectively. When these materials are synthesized in purely OH^- media (i.e., M-MFI-F(0)), more than 90% of the transition-metal atoms within the synthesis gel incorporate into the recovered solids. The amount of metal incorporated, however, decreases monotonically as the concentration of F^- ions increases (Table 1; Figure S8). For example, the percentages of Ti incorporated into Ti-MFI-F(0) and Ti-MFI-F(1.5) are 90 and 13%, respectively. In comparison, 95 and 52% of the Nb atoms are incorporated into Nb-MFI-F(0) and Nb-MFI-F(1.5) materials, respectively, while 90 and 43% of Ta atoms are incorporated into Ta-MFI-F(0) and Ti-MFI-F(1.5), respectively. These trends suggest that F^- ions may react with the transition-metal precursors to form metal fluoride complexes (e.g., $M(OH)_xF_y$; M = Ti, Nb, or Ta) that resist hydrolysis and condensation into the MFI framework. The strong dependence of Ti incorporation efficiency on the HF concentration, relative to Nb or Ta, prompted us to further study how the formation of $Ti(OH)_xF_y$ species depends on HF and Ti concentrations.

The number of Ti atoms incorporated into Ti-MFI-F(1.5) materials also depends on the concentration of the transition-metal precursor within the synthesis gel. Figure 5 shows that

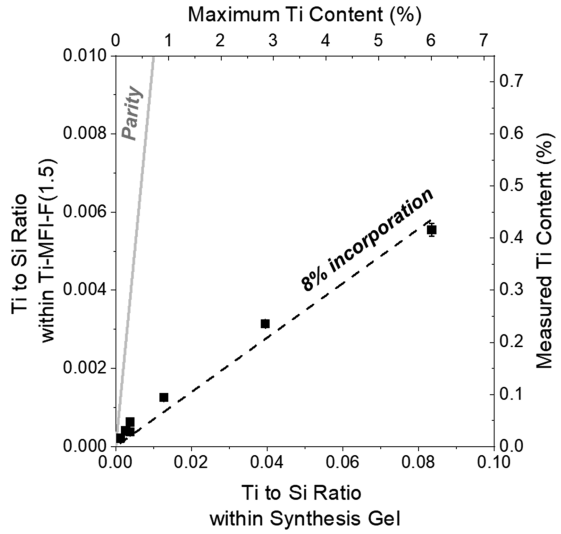

Figure 5. Measured Ti-to-Si ratio within Ti-MFI-F(1.5) as a function of the Ti-to-Si ratio within the synthesis gel. The right and top axes represent the same data plotted as the measured Ti content within Ti-MFI-F(1.5) and the maximum possible Ti content, based upon the synthesis procedure, respectively. The solid gray line represents parity, while the dashed black line is a least-squares regression of the data with an intercept at the origin.

the measured Ti loading within Ti-MFI-F(1.5) increases linearly with the Ti content in the synthesis gel. For all Ti-MFI-F(1.5), the measured Ti content in the recovered solids is ~8% of the Ti content within the synthesis gel. During synthesis, $Ti(OBu)_4$ molecules hydrolyze to form $Ti(OH)_4$ species that condense during crystallization and are incorporated into the MFI framework.[70,71] These $Ti(OH)_4$ species condense via reaction with HF to form stable titanium fluoride complexes ($Ti(OH)_{4-y}F_y$; y = 1−4),[72] which resist framework incorporation. Consequently, the constant ratio of the Ti content within the recovered solids to that in the original synthesis gel likely reflects the equilibrium to form $Ti(OH)_{4-y}F_y$ species, shown in Scheme 3.

^{19}F nuclear magnetic resonance (NMR) and Raman spectroscopy provides direct evidence for the formation of

Scheme 3. Generalized Equilibrium for the Formation of Titanium Fluoride ($Ti(OH)_{4-y}F_y$) Complexes[a]

$$Ti(OH)_4 + y\ HF \overset{K}{\rightleftharpoons} Ti(OH)_{4-y}F_y + y\ H_2O$$

[a]The equilibrium between $Ti(OH)_4$ and HF to form $Ti(OH)_{4-y}F_y$ complexes is generalized to encompass multiple ion-exchange reactions that occur in series (i.e., to form $Ti(OH)_3F$, $Ti(OH)_2F_2$, $Ti(OH)F_3$, and TiF_4).

https://dx.doi.org/10.1021/acs.chemmater.0c02405
Chem. Mater. XXXX, XXX, XXX−XXX

the $Ti(OH)_{4-y}F_y$ complexes. Figure 6 shows that ^{19}F NMR spectra of the supernatant from Si-MFI-F(1.5) and Ti-MFI-F(1.5) contain several features between 80 and 130 ppm. Both supernatants from Si- and Ti-containing syntheses possess ^{19}F NMR features at −130 and −120 ppm, which correspond to solvated $[SiF_6]^{2-}$ and F^- anions, respectively.[73] The supernatant from Ti-MFI-F(1.5) possesses an additional feature at 80 ppm, which has been assigned to solvated $[TiF_6]^{2-}$ complexes.[74] Figure 7a shows Raman spectra of the supernatant from Si-MFI-F(1.5) and Ti-MFI-F(1.5) syntheses, which contain several significant vibrational features between 400 and 700 cm^{-1}. The feature at 470 cm^{-1} corresponds to five- and six-membered ring zeolite precursor units,[75] while the vibration at 570 cm^{-1} is attributed to colloidal MFI particles.[76] The remaining vibrational modes that are common to both Si- and Ti-MFI syntheses, at 510, 555, 605, and 640 cm^{-1}, are associated with the tetrapropylammonium cation.[75,77] Figure 5b shows that the Raman difference spectrum between the supernatant from Ti-MFI-F(1.5) and Si-MFI-F(1.5) contains a single prominent feature at 590 cm^{-1}. Vibrational spectra of homogeneous Ti^{4+} organometallic (e.g., $TiCp_2F_2$) and halogeno (e.g., $TiCl_zF_{4-z}$; z = 0−4) complexes possess ν(Ti−F) modes at 568 cm^{-1}[78] or between 520 and 737 cm^{-1},[79,80] respectively. The feature at 590 cm^{-1} (Figure 7b) does not belong to $Ti(OH)_4$ complexes, which possess ν(Ti−O) between 706 and 752 cm^{-1} (Figure S9 shows the Raman spectra in Figure 5 with an extended abscissa).[81] As such, the vibrational feature at 590 cm^{-1} in Figure 4 likely corresponds to ν(Ti−F) of homogeneous $Ti(OH)_{4-y}F_y$ complexes. These Raman data in conjunction with ^{19}F NMR spectra unambiguously suggest that the formation of soluble titanium fluoride complexes leads to decreased metal incorporation efficiencies.

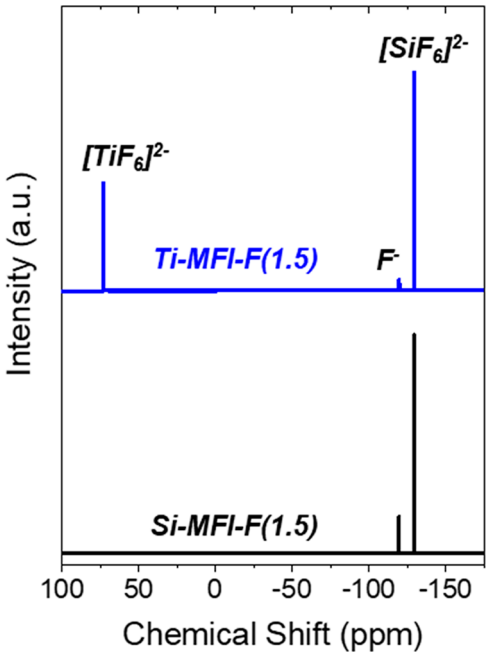

Figure 6. ^{19}F NMR spectra of the supernatant from Ti-MFI-F(1.5) (blue, top) and Si-MFI-F(1.5) (black, bottom) syntheses. The spectra have been normalized to the most intense feature around 130 ppm and are vertically offset for clarity.

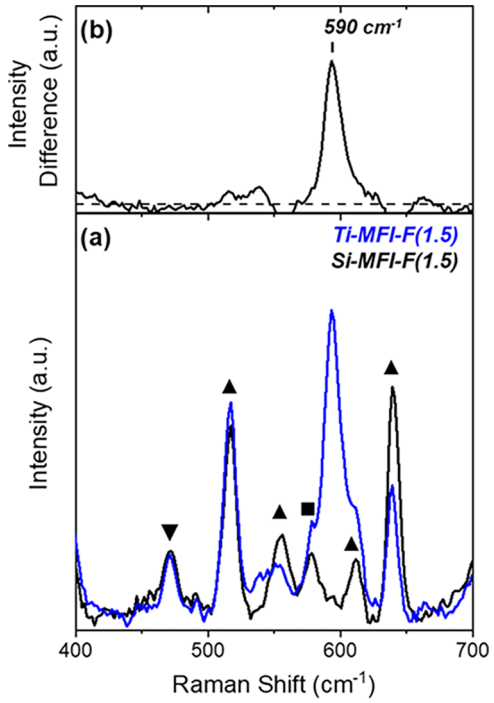

Figure 7. (a) Raman spectra (λ_{ex} = 532 nm) of the dried supernatant from Si-MFI-F(1.5) (black) and Ti-MFI-F(1.5) (blue) syntheses. (b) Difference between the Raman spectra of the dried supernatants from Ti-MFI-F(1.5) and the Si-MFI-F(1.5) syntheses. The dashed black line in (b) represents the baseline. Demarked Raman features correspond to vibrations originating from zeolite precursors (▼), tetrapropylammonium cations (▲), and colloidal MFI particles (■).

Collectively, these data in Sections 3.1 and 3.2 show how the ratio of HF to SDA within a synthesis gel can be used to control the SiOH density by varying the extent of the in situ ion-exchange reaction. The addition of F^- ions, however, also leads to the formation of metal fluoride complexes that do not readily incorporate into the framework.

3.3. Water Sorption and Cluster Sizes Depend on Silanol Density and Heteroatom Identity. The presence and density of polar SiOH functions within a zeolite impact the adsorption of molecules within the pores, which may have implications during catalysis or in separations. Figure 8 shows H_2O vapor adsorption isotherms for Ti-MFI-F(x) and Si-MFI-F(x) materials at 293 K, and adsorption isotherms for Nb- and Ta-MFI-F(x) are shown in Figure S10. H_2O adsorption within M-MFI-F(x) resembles a typical type I isotherm that is characteristic of adsorption within a microporous solid.[82] Figures 8a,b and S10 show that the quantity of H_2O adsorbed at any given P/P_0 increases monotonically with SiOH density regardless of the presence or identity of framework heteroatoms. For example, Si-MFI-F(0) (i.e., synthesized within OH^- media) adsorbs 7 and 100 times more H_2O than Si-MFI-F(1) and Si-MFI-F(1.5) across the entire range of P/P_0 (Figure 6a). The uptakes of H_2O within M-MFI-F(0) are 10−100 times greater than within the corresponding M-MFI-F(1.5) materials (Figures 8 and S10). These comparisons demonstrate the significant effect of SiOH density on the bulk volumetric uptake of H_2O.

Figure 8c shows that the amounts of H_2O adsorbed within Si and Ti-MFI-F(x) are indistinguishable when these structures contain significant densities of SiOH (i.e., where $x \leq 1$). H_2O molecules bind exothermically (∼−33 kJ mol^{-1}) to

https://dx.doi.org/10.1021/acs.chemmater.0c02405
Chem. Mater. XXXX, XXX, XXX−XXX

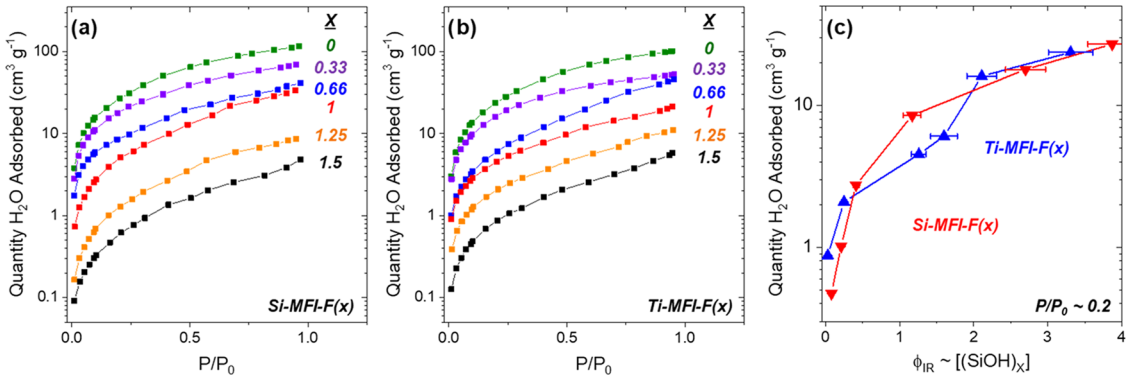

Figure 8. Quantity of H_2O adsorbed as a function of relative H_2O pressures (P/P_0) at 293 K into (a) Si-MFI-F(x) and (b) Ti-MFI-F(x). (c) Quantity of H_2O adsorbed at $P/P_0 = 0.2$ for Ti-MFI-F(x) (blue ▲) and Si-MFI-F(x) (red ▼) plotted against the values of ϕ_{IR} (i.e., a measure of SiOH density). Within panels (a) and (b), refer to the color-coded legend for each HF-to-TPAOH ratio. Adsorption isotherms are not vertically offset.

monomeric, dimeric, and oligomeric H_2O clusters,[83] which indicates that H_2O clusters form spontaneously within materials that contain significant densities of SiOH upon coordination of a single H_2O. In contrast, Si-MFI-F(x) that contain few SiOH (i.e., where $x \geq 1.25$) adsorbs significantly less H_2O than the corresponding Ti-MFI-F(x), which suggests that framework Ti atoms serve to nucleate and bind a non-negligible number of H_2O molecules.

To examine the interactions between adsorbed H_2O molecules and framework metal atoms, we accounted for the contributions from SiOH functions by subtracting the adsorption isotherm of Si-MFI-F(x) from those of Ti-, Nb-, or Ta-MFI-F(x) (where x = 1, 1.25, or 1.5). The particular M-MFI-F(x) in this analysis were chosen because their ϕ_{IR} values are within 0.05 of the corresponding Si-MFI-F(x), which was important to deconvolute H_2O adsorption to heteroatoms from adsorption onto SiOH defects. Figure 9 shows the number of H_2O molecules adsorbed per metal atom within M-MFI-F(x) as a function of H_2O pressure. Importantly, H_2O adsorption isotherms normalized per Ti or Nb atom are indistinguishable for a given metal, which suggests that these data reflect H_2O adsorption solely to framework heteroatoms.[84] For all M-MFI-F(x), the average number of H_2O molecules bound to framework M atoms increases monotonically as the pressure of H_2O increases from 0.02 to 2.3 kPa. At all H_2O vapor pressures, the uptake of H_2O at Nb or Ta atoms is greater than at Ti atoms, which suggests that H_2O binds more exothermically to Nb or Ta atoms than to Ti.

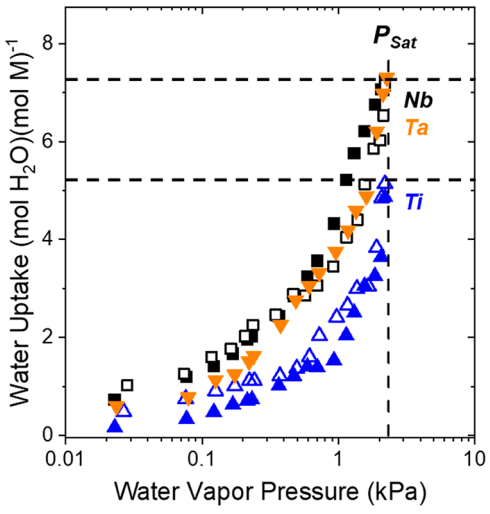

Figure 9. Mean number of water molecules bound to framework heteroatoms (Ti, Nb) in MFI as a function of H_2O vapor pressure at 293 K for Ti-MFI-F(1.25) (blue △), Ti-MFI-F(1.5) (blue ▲), Nb-MFI-F(1) (black □), Nb-MFI-F(1.5) (black ■), or Ta-MFI-F(1.5) (orange ▼). Values are calculated from the difference between the H_2O uptake on a given material and Si-MFI-F(x), which is then normalized by the number of metal atoms. The saturation vapor pressure of H_2O (P_{Sat}) at 293 K is 2.34 kPa.

At equilibrium, the chemical potential of H_2O within the vapor phase equals that of H_2O bound to M atoms. Further, the chemical potential of H_2O within the liquid and vapor phases is equal at the saturation vapor pressure (P_{Sat}; 2.34 kPa, 293 K). Consequently, the number of H_2O atoms adsorbed at an M atom at the saturation pressure of H_2O represents the size of the solvent structure that would form when the zeolite is immersed within liquid H_2O. This reasoning, combined with the result in Figure 9, shows that Nb and Ta atoms stabilize approximately 7−8 H_2O molecules within aqueous media (i.e., at P_{Sat}). In comparison, recent work shows that Brønsted acid sites within H^+-Al-MFI stabilize 8 H_2O molecules in liquid H_2O, within a structure that consists of a hydronium cation (H_3O^+) surrounded by a seven-membered solvation shell.[24] Nb and Ta atoms substituted within the framework of a zeolite exist as $M(OSi)_4OH$,[6,49,85,86] which acts as a weak Brønsted acid as shown from the vibrational spectra of adsorbed pyridine. The similarities in H_2O cluster size within Nb- and Ta-MFI-F(1.5) and those within H^+-Al-MFI[24] suggest that 7−8 H_2O molecules solvate protic sites within the MFI framework, regardless of the identity of the associated framework heteroatom.

In contrast to Nb, Ta, and Al atoms, framework-substituted Ti atoms exist as $Ti(OSi)_4$ and are Lewis acidic and not Bronsted acidic.[8,12,87] Figure 9 shows that Ti atoms would stabilize ~5 H_2O molecules within liquid H_2O (i.e., at P_{Sat}). Recent work with ab initio molecular dynamics simulations showed that interactions between H_2O and Lewis acidic Sn sites (i.e., $Sn(OSi)_4$ and $Si(OSi)_3OH$) within Sn-BEA zeolites stabilize small H_2O clusters that comprise 5−6 H_2O molecules.[13] Notably, the binding energy of H_2O to a framework Sn atom is greater than to a Ti atom (i.e., −32 versus −12 kJ mol^{-1} for Sn- and Ti-BEA, respectively).[88] As such, the size of the H_2O structures that form at Lewis acid sites appears to be weakly dependent on the size of the

https://dx.doi.org/10.1021/acs.chemmater.0c02405
Chem. Mater. XXXX, XXX, XXX−XXX

surrounding microporous cavity (MFI and BEA have average pore diameters of 0.55 and 0.65 nm, respectively)[6] and the binding energy of H_2O to the Lewis acid site. Collectively, these data and interpretations suggest that H_2O structures formed at Lewis acid sites (~5 H_2O per Lewis acidic M atom) are distinct from those formed at Brønsted acid sites (~7−8 H_2O per H^+), which may have implications in the performance of a zeolite as a catalyst or adsorbent.

The structure of H_2O molecules within a zeolite pore greatly influences the thermodynamic stability of surface intermediates, which drastically affects catalysis.[11,12,89,90] Rates of alkene epoxidation over Ti-BEA increase by a factor of 100 between nearly defect-free materials and Ti-BEA that contain ~5 $(SiOH)_4$ per unit cell.[11,12] Ti-BEA that contain high densities of $(SiOH)_4$ nucleate H_2O structures near Ti active sites. These H_2O structures reorganize during catalysis and contribute to large increases in the excess entropy that ultimately increase the rates of 1-octene epoxidation. In contrast, SiOH-rich domains within Ti- and Sn-BEA inhibit aqueous-phase glucose isomerization.[8,32] Ti- and Sn-BEA that contain significant SiOH densities stabilize hydrogen-bonded H_2O networks; in contrast, hydrophobic materials contain gas-like molecular H_2O structures. The exclusion and reorganization of these H_2O molecules contribute to changes in the apparent free energies of activation, which lead to decreased rates of glucose isomerization in hydrophilic catalysts.[8] In the context of adsorption, both hydrophilic and hydrophobic H-ZSM-5 adsorb comparable amounts of ethanol, while hydrophilic materials adsorb 4 times more H_2O than within hydrophobic pores,[18] which shows the potential for selective separations within aqueous alcohol mixtures. Recently, Gould et al. constructed a Born−Haber thermochemical cycle to assess the effects of confinement and solvation on pyridine adsorption in Brønsted acid zeotypes (MFI, BEA, FAU, SBA-15, MCM-41), and this analysis showed that the apparent free energies for an adsorption process depend strongly on the structure of the solvating molecules.[90] We have recently taken a similar approach to determine the significance of individual types of interactions on free-energy landscapes for alkene epoxidations in liquid-filled pores of Ti-silicates.[12,91] These findings demonstrate that distinct contributions to the free energy of activation by solvent restructuring and inner-sphere interactions among reactive surface species lead to changes in epoxidation rates in excess of 1000-fold. These studies, a portion of the literature, exemplify how the structure of solvent molecules within microporous solids can lead to large changes in catalytic rates or separation selectivities.

Collectively, these results show how the HF/SDA ratio within the synthesis gel can be varied to control the density of SiOH groups within the recovered zeolite materials. This simple method can likely be extended to other zeolite frameworks and heteroatom identities, which will enable researchers to access materials with tunable properties to study the effects of complex interactions at the solid−liquid interface on catalysis and separation processes.

4. CONCLUSIONS

The density of polar SiOH functions within siliceous and heteroatom-substituted MFI zeolites (M = Ti, Nb, and Ta) can be controlled by tuning the ratio of HF to TPAOH (from 0 to 2) within the synthesis gel. The relative densities of SiOH groups, characterized by infrared spectroscopy, decrease linearly with the HF/TPAOH ratio and approach zero at an HF/TPAOH ratio of 1.5. HF and TPAOH ion exchange in situ to form TPAF, which does not lead to the formation of anionic vacancy defects in the final zeolite. Consequently, the use of HF in excess of TPAOH is necessary to produce materials without SiOH defects, because this ion exchange is dictated by equilibrium. Metal fluoride complexes (e.g., $Ti(OH)_xF_y$) formed by the reaction of $Ti(OH)_4$ with HF resist framework incorporation and lead to significant fractions of metal ions (e.g., Ti^{4+}) that do not end up in the final zeolite. The low amounts of metal incorporation, however, can be mitigated by using a greater amount of metal precursor, as the metal loading in the recovered materials depends linearly on the concentration of the metal precursor within the synthesis gel.

Vapor-phase H_2O adsorption shows that M-MFI materials synthesized with an HF/TPAOH ratio of 1.5 adsorb 10−100 times less H_2O than those synthesized in the absence of HF, which far exceeds the 4-fold difference reported in conventional hydrophilic and hydrophobic MFI zeolites. Comparisons of H_2O adsorption within defect-free materials reveal that Ti and Nb atoms selectively stabilize H_2O clusters that are 5 and 7−8 H_2O molecules in size, respectively. Nb and Ta atoms exist with a pendant hydroxyl (M-OH), which suggests that these adsorption sites behave similarly to Brønsted acids. In contrast, Lewis acid sites nucleate structurally distinct H_2O structures that do not appear to depend strongly on the identity of the heteroatom (Ti versus Sn) or size of the surrounding micropore (MFI versus BEA). The formation of specific solvent structures at heteroatoms within zeolites may have significant implications in catalysis and adsorption processes, which are ongoing investigations within our group. Collectively, this work presents a robust synthetic method for producing heteroatom-substituted zeolites with precise control over the density of SiOH groups.

■ ASSOCIATED CONTENT

Supporting Information

The Supporting Information is available free of charge at https://pubs.acs.org/doi/10.1021/acs.chemmater.0c02405.

X-ray diffractograms, diffuse reflectance UV−vis spectra, infrared spectra, H_2O adsorption isotherms, and Raman spectra (PDF)

■ AUTHOR INFORMATION

Corresponding Author

David W. Flaherty − *Department of Chemical and Biomolecular Engineering, University of Illinois at Urbana-Champaign, Urbana, Illinois 61801, United States;* orcid.org/0000-0002-0567-8481; Email: dwflhrty@illinois.edu

Authors

Daniel T. Bregante − *Department of Chemical and Biomolecular Engineering, University of Illinois at Urbana-Champaign, Urbana, Illinois 61801, United States;* orcid.org/0000-0003-2157-1286

David S. Potts − *Department of Chemical and Biomolecular Engineering, University of Illinois at Urbana-Champaign, Urbana, Illinois 61801, United States;* orcid.org/0000-0001-8303-7359

https://dx.doi.org/10.1021/acs.chemmater.0c02405
Chem. Mater. XXXX, XXX, XXX−XXX

Ohsung Kwon − *Department of Chemical and Biomolecular Engineering, University of Illinois at Urbana-Champaign, Urbana, Illinois 61801, United States*
E. Zeynep Ayla − *Department of Chemical and Biomolecular Engineering, University of Illinois at Urbana-Champaign, Urbana, Illinois 61801, United States*
Jun Zhi Tan − *Department of Chemical and Biomolecular Engineering, University of Illinois at Urbana-Champaign, Urbana, Illinois 61801, United States*

Complete contact information is available at: https://pubs.acs.org/10.1021/acs.chemmater.0c02405

Notes

The authors declare the following competing financial interest(s): D.T.B. and D.W.F. are inventors on a patent application for the synthesis and application of heteroatom-substituted zeolites of varying silanol density, submitted by the University of Illinois at Urbana-Champaign.

■ ACKNOWLEDGMENTS

We thank Dr. Lingyang Zhu for technical assistance in acquiring ^{19}F NMR spectra. D.T.B. was supported by a dissertation completion fellowship through the University of Illinois. E.Z.A. was supported by the Army Research Office (W911NF-18-1-0100). This work was carried out, in part, in the Frederick Seitz Materials Research Laboratory Central Research Facilities and the School of Chemical Sciences NMR Lab, both at the University of Illinois. This work was supported by the Department of Energy, Office of Science, Office of Basic Energy Sciences, under Award DE-SC0020224.

■ REFERENCES

(1) Gounder, R.; Iglesia, E. The catalytic diversity of zeolites: confinement and solvation effects within voids of molecular dimensions. *Chem. Commun.* **2013**, *49*, 3491−3509.
(2) Davis, M. E. New Vistas in Zeolite and Molecular Sieve Catalysis. *Acc. Chem. Res.* **1993**, *26*, 111−115.
(3) Jones, C. W.; Tsuji, K.; Davis, M. E. Organic-functionalized molecular sieves as shape-selective catalysts. *Nature* **1998**, *393*, 52−54.
(4) Corma, A. State of the art and future challenges of zeolites as catalysts. *J. Catal.* **2003**, *216*, 298−312.
(5) Hill, J. R.; Sauer, J. Molecular Mechanics Potential for Silica and Zeolite Catalysts Based on ab Initio Calculations. 1. Dense and Microporous Silica. *J. Phys. Chem. A* **1994**, *98*, 1238−1244.
(6) Bregante, D. T.; Tan, J. Z.; Sutrisno, A.; Flaherty, D. W. Heteroatom substituted zeolite FAU with ultralow Al contents for liquid-phase oxidation catalysis. *Catal.: Sci. Technol.* **2020**, *10*, 635−647.
(7) Bregante, D. T.; Thornburg, N. E.; Notestein, J. M.; Flaherty, D. W. Consequences of Confinement for Alkene Epoxidation with Hydrogen Peroxide on Highly Dispersed Group 4 and 5 Metal Oxide Catalysts. *ACS Catal.* **2018**, *8*, 2995−3010.
(8) Cordon, M. J.; Harris, J. W.; Vega-Vila, J. C.; Bates, J. S.; Gupta, M.; Witzke, M. E.; Wegener, E. C.; Miller, J. T.; Flaherty, D. W.; Hibbitts, D. D.; Gounder, R.; et al. The Dominant Role of Entropy in Stabilizing Sugar Isomerization Transition States within Hydrophobic Zeolite Pores. *J. Am. Chem. Soc.* **2018**, *140*, 14244−14266.
(9) Harris, J. W.; Cordon, M. J.; Di Iorio, J. R.; Vega-Vila, J. C.; Ribeiro, F. H.; Gounder, R. Titration and quantification of open and closed Lewis acid sites in Sn-Beta zeolites that catalyze glucose isomerization. *J. Catal.* **2016**, *335*, 141−154.
(10) Bates, J. S.; Gounder, R. Influence of confining environment polarity on ethanol dehydration catalysis by Lewis acid zeolites. *J. Catal.* **2018**, *365*, 213−226.
(11) Bregante, D. T.; Johnson, A. M.; Patel, A. Y.; Ayla, E. Z.; Cordon, M. J.; Bukowski, B. C.; Greeley, J.; Gounder, R.; Flaherty, D. W. Cooperative Effects between Hydrophilic Pores and Solvents: Catalytic Consequences of Hydrogen Bonding on Alkene Epoxidation in Zeolites. *J. Am. Chem. Soc.* **2019**, *141*, 7302−7319.
(12) Bregante, D. T.; Flaherty, D. W. Impact of Specific Interactions Among Reactive Surface Intermediates and Confined Water on Epoxidation Catalysis and Adsorption in Lewis Acid Zeolites. *ACS Catal.* **2019**, *9*, 10951−10962.
(13) Bukowski, B. C.; Bates, J. S.; Gounder, R.; Greeley, J. Defect-Mediated Ordering of Condensed Water Structures in Microporous Zeolites. *Angew. Chem., Int. Ed.* **2019**, *58*, 16422−16426.
(14) Bukowski, B. C.; Bates, J. S.; Gounder, R.; Greeley, J. First principles, microkinetic, and experimental analysis of Lewis acid site speciation during ethanol dehydration on Sn-Beta zeolites. *J. Catal.* **2018**, *365*, 261−276.
(15) Khouw, C. B.; Dartt, C. B.; Labinder, J. A.; Davis, M. E. Studies on the Catalytic Oxidation of Alkanes and Alkenes by Titanium Silicates. *J. Catal.* **1994**, *149*, 195−205.
(16) Blasco, T.; Camblor, M. A.; Corma, A.; Esteve, P.; Guil, J. M.; Martinez, A.; Perdigon-Melon, J. A.; Valencia, S. Direct synthesis and characterization of hydrophobic aluminum-free Ti-beta zeolite. *J. Phys. Chem. B* **1998**, *102*, 75−88.
(17) Gounder, R.; Davis, M. E. Monosaccharide and disaccharide isomerization over Lewis acid sites in hydrophobic and hydrophilic molecular sieves. *J. Catal.* **2013**, *308*, 176−188.
(18) Zhang, K.; Lively, R. P.; Noel, J. D.; Dose, M. E.; McCool, B. A.; Chance, R. R.; Koros, W. J. Adsorption of water and ethanol in MFI-type zeolites. *Langmuir* **2012**, *28*, 8664−8673.
(19) Grieneisen, J. L.; Kessler, H.; Fache, E.; Le Govic, A. M. Synthesis of TS-1 in fluoride medium. A new way to a cheap and efficient catalyst for phenol hydroxylation. *Microporous Mesoporous Mater.* **2000**, *37*, 379−386.
(20) Caullet, P.; Paillaud, J.-L.; Simon-Masseron, A.; Soulard, M.; Patarin, J. The fluoride route: a strategy to crystalline porous materials. *C. R. Chim.* **2005**, *8*, 245−266.
(21) Chezeau, J. M.; Delmotte, L.; Guth, J. L.; Gabelica, Z. Influence of synthesis conditions and postsynthesis treatments ont he nature and quantity of structure defects in highly siliceous MFI zeolites: A high-resolution solid-state 29Si NMR study. *Zeolites* **1991**, *11*, 598−606.
(22) DeJaco, R. F.; de Mello, M. D.; Nguyen, H. G. T.; Jeon, M. Y.; Zee, R. D.; Tsapatsis, M.; Siepmann, J. I. Vapor- and liquid-phase adsorption of alcohol and water in silicalite-1 synthesized in fluoride media. *AlChE J.* **2020**, *66*, No. e16868.
(23) Mallon, E. E.; Jeon, M. Y.; Navarro, M.; Bhan, A.; Tsapatsis, M. Probing the relationship between silicalite-1 defects and polyol adsorption properties. *Langmuir* **2013**, *29*, 6546−6555.
(24) Eckstein, S.; Hintermeier, P. H.; Zhao, R.; Barath, E.; Shi, H.; Liu, Y.; Lercher, J. A. Influence of Hydronium Ions in Zeolites on Sorption. *Angew. Chem., Int. Ed.* **2019**, *58*, 3450−3455.
(25) Qin, Z.; Lakiss, L.; Tosheva, L.; Gilson, J.-P.; Vicente, A.; Fernandez, C.; Valtchev, V. Comparative Study of Nano-ZSM-5 Catalysts Synthesized in OH−and F−Media. *Adv. Funct. Mater.* **2014**, *24*, 257−264.
(26) Grahn, M.; Faisal, A.; Öhrman, O. G. W.; Zhou, M.; Signorile, M.; Crocellà, V.; Nabavi, M. S.; Hedlund, J. Small ZSM-5 crystals with low defect density as an effective catalyst for conversion of methanol to hydrocarbons. *Catal. Today* **2020**, *345*, 136−146.
(27) Grosso-Giordano, N. A.; Schroeder, C.; Okrut, A.; Solovyov, A.; Schottle, C.; Chasse, W.; Marinkovic, N.; Koller, H.; Zones, S. I.; Katz, A. Outer-Sphere Control of Catalysis on Surfaces: A Comparative Study of Ti(IV) Single-Sites Grafted on Amorphous versus Crystalline Silicates for Alkene Epoxidation. *J. Am. Chem. Soc.* **2018**, *140*, 4956−4960.
(28) Grosso-Giordano, N. A.; Hoffman, A. S.; Boubnov, A.; Small, D. W.; Bare, S. R.; Zones, S. I.; Katz, A. Dynamic Reorganization and Confinement of Ti(IV) Active Sites Controls Olefin Epoxidation

Catalysis on Two-Dimensional Zeotypes. *J. Am. Chem. Soc.* **2019**, *141*, 7090−7106.
(29) Wang, L.; Sun, J.; Meng, X.; Zhang, W.; Zhang, J.; Pan, S.; Shen, Z.; Xiao, F. S. A significant enhancement of catalytic activities in oxidation with H2O2 over the TS-1 zeolite by adjusting the catalyst wettability. *Chem. Commun.* **2014**, *50*, 2012−2014.
(30) Wang, M.; Jaegers, N. R.; Lee, M.-S.; Wan, C.; Hu, J. Z.; Shi, H.; Mei, D.; Burton, S. D.; Camaioni, D. M.; Gutierrez, O. Y.; Glezakou, V.-A.; Rousseau, R.; Wang, Y.; Lercher, J. A. Genesis and Stability of Hydronium Ions in Zeolite Channels. *J. Am. Chem. Soc.* **2019**, *141*, 3444−3455.
(31) Conrad, S.; Wolf, P.; Müller, P.; Orsted, H.; Hermans, I. Influence of Hydrophilicity on the Snβ-Catalyzed Baeyer-Villiger Oxidation of Cyclohexanone with Aqueous Hydrogen Peroxide. *ChemCatChem* **2017**, *9*, 175−182.
(32) Vega-Vila, J. C.; Harris, J. W.; Gounder, R. Controlled insertion of tin atoms into zeolite framework vacancies and consequences for glucose isomerization catalysis. *J. Catal.* **2016**, *344*, 108−120.
(33) Cho, H. J.; Gould, N. S.; Vattipalli, V.; Sabnis, S.; Chaikittisilp, W.; Okubo, T.; Xu, B.; Fan, W. Fabrication of hierarchical Lewis acid Sn-BEA with tunable hydrophobicity for cellulosic sugar isomerization. *Microporous Mesoporous Mater.* **2019**, *278*, 387−396.
(34) Bai, P.; Siepmann, J. I.; Deem, M. W. Adsorption of glucose into zeolite beta from aqueous solution. *AlChE J.* **2013**, *59*, 3523−3529.
(35) Gounder, R. Hydrophobic microporous and mesoporous oxides as Brønsted and Lewis acid catalysts for biomass conversion in liquid water. *Catal.: Sci. Technol.* **2014**, *4*, 2877−2886.
(36) Lobo, R. F.; Zones, S. I.; Davis, M. E. Structure-Direction in Zeolite Synthesis. *J. Inclusion Phenom. Mol. Recognit. Chem.* **1995**, *21*, 47−78.
(37) Moliner, M.; Rey, F.; Corma, A. Towards the rational design of efficient organic structure-directing agents for zeolite synthesis. *Angew. Chem., Int. Ed.* **2013**, *52*, 13880−13889.
(38) Li, J.; Corma, A.; Yu, J. Synthesis of new zeolite structures. *Chem. Soc. Rev.* **2015**, *44*, 7112−7127.
(39) Archer, R. H.; Zones, S. I.; Davis, M. E. Imidazolium structure directing agents in zeolite synthesis: Exploring guest/host relationships in the synthesis of SSZ-70. *Microporous Mesoporous Mater.* **2010**, *130*, 255−265.
(40) Moliner, M.; Martinez, C.; Corma, A. Multipore zeolites: synthesis and catalytic applications. *Angew. Chem., Int. Ed.* **2015**, *54*, 3560−3579.
(41) Gounder, R.; Davis, M. E. Beyond shape selective catalysis with zeolites: Hydrophobic void spaces in zeolites enable catalysis in liquid water. *AlChE J.* **2013**, *59*, 3349−3358.
(42) Guth, J. L.; Kessler, H.; Higel, J. M.; Lamblin, J. M.; Patarin, J.; Seive, A.; Chezeau, J. M.; Way, R. Zeolite Synthesis in the Presence of Fluoride Ions. *ACS Symp. Ser.* **1989**, *398*, 176−195.
(43) Corma, A.; Camblor, M. A.; Esteve, P.; Martínez, A.; Perez-Pariente, J. Activity of Ti-Beta Catalyst for the Selective Oxidation of Alkenes and Alkanes. *J. Catal.* **1994**, *145*, 151−158.
(44) Ikeue, K.; Yamashita, H.; Anpo, M.; Takewaki, T. Photocatalytic Reduction of CO_2 with H_2O on Ti-Beta Zeolite Photocatalysts: Effect of the Hydrophobic and Hydrophilic Properties. *J. Phys. Chem. B* **2001**, *105*, 8350−8355.
(45) Cordon, M. J.; Harris, J. W.; Vega-Vila, J. C.; Bates, J. S.; Kaur, S.; Gupta, M.; Witzke, M. E.; Wegener, E. C.; Miller, J. T.; Flaherty, D. W.; Hibbitts, D. D.; Gounder, R. Dominant Role of Entropy in Stabilizing Sugar Isomerization Transition States within Hydrophobic Zeolite Pores. *J. Am. Chem. Soc.* **2018**, *140*, 14244−14266.
(46) Cordon, M. J.; Hall, J. N.; Harris, J. W.; Bates, J. S.; Hwang, S.-J.; Gounder, R. Deactivation of Sn-Beta zeolites caused by structural transformation of hydrophobic to hydrophilic micropores during aqueous-phase glucose isomerization. *Catal.: Sci. Technol.* **2019**, *9*, 1654−1668.
(47) Han, S. W.; Kim, J.; Ryoo, R. Dry-gel synthesis of mesoporous MFI zeolite nanosponges using a structure-directing surfactant. *Microporous Mesoporous Mater.* **2017**, *240*, 123−129.
(48) Bregante, D. T.; Patel, A. Y.; Johnson, A. M.; Flaherty, D. W. Catalytic Thiophene Oxidation by Groups 4 and 5 Framework-Substituted Zeolites with Hydrogen Peroxide: Mechanistic and Spectroscopic Evidence for the Effects of Metal Lewis Acidity and Solvent Lewis Basicity. *J. Catal.* **2018**, *364*, 415−425.
(49) Dzwigaj, S.; Millot, Y.; Méthivier, C.; Che, M. Incorporation of Nb(V) into BEA zeolite investigated by XRD, NMR, IR, DR UV−vis, and XPS. *Microporous Mesoporous Mater.* **2010**, *130*, 162−166.
(50) Bai, P.; Tsapatsis, M.; Siepmann, J. I. Multicomponent adsorption of alcohols onto silicalite-1 from aqueous solution: isotherms, structural analysis, and assessment of ideal adsorbed solution theory. *Langmuir* **2012**, *28*, 15566−15576.
(51) Ramachandran, C.; Du, H.; Kim, Y.; Kung, M.; Snurr, R.; Broadbelt, L. Solvent effects in the epoxidation reaction of 1-hexene with titanium silicalite-1 catalyst. *J. Catal.* **2008**, *253*, 148−158.
(52) Lechert, H. The pH-value and its importance for the crystallization of zeolites. *Verified Synth. Zeolitic Mater.* **2001**, 33−38.
(53) Fegan, S. G.; Lowe, B. M. Effect of Alkalinity on the Crystallization of Silicalite-1 Precursors. *J. Chem. Soc., Faraday Trans. 1* **1986**, *82*, 785−799.
(54) Corma, A.; Llabre's i Xamena, F. X.; Prestipino, C.; Renz, M.; Valencia, S. Water Resistant, Catalytically Active Nb and Ta Isolated Lewis Acid Sites, Homogeneously Distributed by Direct Synthesis in a Beta Zeolite. *J. Phys. Chem. C* **2009**, *113*, 11306−11315.
(55) Corma, A.; Nemeth, L.; Renz, M.; Valencia, S. Sn-zeolite beta as a heterogeneous chemoselective catalytic for Baeyer-Villiger oxidations. *Nature* **2001**, *412*, 423−425.
(56) International Zeolite Association. Verified Syntheses of Zeolitic Materials: Characterization by IR Spectroscopy. http://www.izaonline.org/synthesis/VS_2ndEd/IR_Spectroscopy.htm (accessed August 1, 2020).
(57) Thornburg, N. E.; Thompson, A. B.; Notestein, J. M. Periodic Trends in Highly Dispersed Groups IV and V Supported Metal Oxide Catalysts for Alkene Epoxidation with H_2O_2. *ACS Catal.* **2015**, *5*, 5077−5088.
(58) Klaas, J.; Schulz-Ekloff, G.; Jaeger, N. I. UV-Visible Diffuse Reflectance Spectroscopy of Zeolite-Hosted Mononuclear Titanium Oxide Species. *J. Phys. Chem. B* **1997**, *101*, 1305−1311.
(59) Dzwigaj, S.; Millot, Y.; Che, M. Ta(V)-Single Site BEA Zeolite by Two-Step Postsynthesis Method: Preparation and Characterization. *Catal. Lett.* **2010**, *135*, 169−174.
(60) Zhao, Y.; Zhou, X.; Ye, L.; Tsang, S. C. E. Nanostructured Nb_2O_5 catalysts. *Nano Rev.* **2012**, *3*, No. 17631.
(61) Chun, W.; Ishikawa, A.; Fujisawa, H.; Takata, T.; Kondo, J. N.; Hara, M.; Kawai, M.; Matsumoto, Y.; Domen, K. Conduction and Valence Band Positions of Ta_2O_5, TaON, and Ta3N5 by UPS and Electrochemical Methods. *J. Phys. Chem. B* **2003**, *107*, 1798−1803.
(62) Prodinger, S.; Derewinski, M. A.; Vjunov, A.; Burton, S. D.; Arslan, I.; Lercher, J. A. Improving Stability of Zeolites in Aqueous Phase via Selective Removal of Structural Defects. *J. Am. Chem. Soc.* **2016**, *138*, 4408−4415.
(63) Wolf, P.; Hammond, C.; Conrad, S.; Hermans, I. Post-synthetic preparation of Sn-, Ti- and Zr-beta: a facile route to water tolerant, highly active Lewis acidic zeolites. *Dalton Trans.* **2014**, *43*, 4514−4519.
(64) Sayed, M. B.; Kydd, R. A.; Cooney, R. P. A Fourier-Transform Infrared Spectral Study of H-ZSM-5 Surface Sites and Reactivity Sequences in Methanol Conversion. *J. Catal.* **1984**, *88*, 137−149.
(65) Eilertsen, E. A.; Arstad, B.; Svelle, S.; Lillerud, K. P. Single parameter synthesis of high silica CHA zeolites from fluoride media. *Microporous Mesoporous Mater.* **2012**, *153*, 94−99.
(66) Di Iorio, J. R.; Gounder, R. Controlling the Isolation and Pairing of Aluminum in Chabazite Zeolites Using Mixtures of Organic and Inorganic Structure-Directing Agents. *Chem. Mater.* **2016**, *28*, 2236−2247.
(67) Ivanova, S.; Lebrun, C.; Vanhaecke, E.; Pham-Huu, C.; Louis, B. Influence of the zeolite synthesis route on its catalytic properties in the methanol to olefin reaction. *J. Catal.* **2009**, *265*, 1−7.

https://dx.doi.org/10.1021/acs.chemmater.0c02405
Chem. Mater. XXXX, XXX, XXX−XXX

(68) Moliner, M.; Corma, A. Synthesis of Expanded Titanosilicate MWW-Related Materials from a Pure Silica Precursor. *Chem. Mater.* **2012**, *24*, 4371−4375.
(69) Barrett, P. A.; Diaz-Cabanas, M. J.; Comblor, M. A.; Jones, R. H. Synthesis in fluoride and hydroxide media and structure of the extra-large pore pure silica zeolite CIT-5. *Faraday Trans.* **1998**, *94*, 2475−2481.
(70) Ricchiardi, G.; de Man, A.; Sauer, J. The effect of hydration on structure and location of Ti-sites in Ti-silicalite catalysts. A computational study. *Phys. Chem. Chem. Phys.* **2000**, *2*, 2195−2204.
(71) Wu, R.; Zhang, C.; Zhao, J.; Bai, Y. Synthesis and characterization of Cr-containing silica gel and Ti-containing silica gel. *J. Ceram. Process. Res.* **2014**, *15*, 433−440.
(72) Decken, A.; Ilyin, E. G.; Brooke Jenkins, H. D.; Nikiforov, G. B.; Passmore, J. Hexafluoroantimony(V) salts of the cationic Ti(IV) fluoride non metallocene complexes $[TiF_3(MeCN)_3]^+$ and $[TiF_2L]^{2+}$ (L = 15-Crown-5 and 18-Crown-6). Preparation, characterization and thermodynamic stability. *Dalton Trans.* **2005**, 3039−3050.
(73) Finney, W. F.; Wilson, E.; Callender, A.; Morris, M. D.; Beck, L. W. Reexamination of Hexafluorosilicate Hydrolysis by 19F NMR and pH Measurement. *Environ. Sci. Technol.* **2006**, *40*, 2572−2577.
(74) Serre, C.; Corbière, T.; Lorentz, C.; Taulelle, F.; Férey, G. Hydrothermal Synthesis of Nanoporous Metalofluorophosphates. 1. Precursor Solutions of Titanium Fluroide and Fluorophosphate in Water, a ^{19}F and ^{31}P NMR Study. *Chem. Mater.* **2002**, *14*, 4939−4947.
(75) Dutta, P. K.; Puri, M. Synthesis and Structure of Zeolite ZSM-5: A Raman Spectroscopic Study. *J. Phys. Chem. B* **1987**, *91*, 4329−4333.
(76) Kirschhock, C. E. A.; Ravishankar, R.; Verspeurt, F.; Grobert, P. J.; Jacobs, P. A.; Martens, J. A. Identification of Precursor Species in the Formation of MFI Zeolite in the TPAOH-TEOS-H2O System. *J. Phys. Chem. B* **1999**, *103*, 4965−4971.
(77) Schmidt, J. E.; Fu, D.; Deem, M. W.; Weckhuysen, B. M. Template-Framework Interactions in Tetraethylammonium-Directed Zeolite Synthesis. *Angew. Chem., Int. Ed.* **2016**, *55*, 16044−16048.
(78) Maslowsky, E.; Nakamoto, K. Vibrational Spectra of Tetrahedral Cyclopentadienyl Halogeno Complexes of Ti(IV) and Zr(IV). *Appl. Spectrosc.* **1971**, *25*, 187−191.
(79) Bauschlicher, C. W.; Taylor, P. R.; Komornicki, A. The vibrational frequencies of $TiFnCl_{4-n}$, n=0,4. *J. Chem. Phys.* **1990**, *92*, 3982−3984.
(80) Clark, R. J. H.; Errington, W. Fluoro-complexes of group IVa Elements: Metal-Halogen Vibrational Frequencies. *J. Chem. Soc. A* **1967**, 258−261.
(81) Ignatyev, I. S.; Montejo, M.; Gonzalez, J. J. L. Structure and Vibrational Spectra of Ti(IV) Hydroxides and Their Clusters with Expanded Titanium Coordination. DFT Study. *J. Phys. Chem. A* **2007**, *111*, 7973−7979.
(82) Thommes, M.; Kaneko, K.; Neimark, A. V.; Olivier, J. P.; Rodriguez-Reinoso, F.; Rouquerol, J.; Sing, K. S. W. Physisorption of gases, with special reference to the evaluation of surface area and pore size distribution (IUPAC Technical Report). *Pure Appl. Chem.* **2015**, *87*, 1051−1069.
(83) Shields, R. M.; Temelso, B.; Archer, K. A.; Morrell, T. E.; Shields, G. C. Accurate Predictions of Water Cluster Formation, $(H_2O)_n$ n=2-10. *J. Phys. Chem. A* **2010**, *114*, 11725−11737.
(84) The similarities in water adsorption isotherms normalized by framework heteroatoms, for a given metal atom, suggests that any small temperature fluctuations during these experiments do not significantly affect the measured isotherms.
(85) Bregante, D. T.; Priyadarshini, P.; Flaherty, D. W. Kinetic and spectroscopic evidence for reaction pathways and intermediates for olefin epoxidation on Nb in * BEA. *J. Catal.* **2017**, *348*, 75−89.
(86) Bregante, D. T.; Flaherty, D. W. Periodic Trends in Olefin Epoxidation over Group IV and V Framework Substituted Zeolite Catalysts: A Kinetic and Spectroscopic Study. *J. Am. Chem. Soc.* **2017**, *139*, 6888−6898.
(87) Gunther, W. R.; Michaelis, V. K.; Griffin, R. G.; Román-Leshkov, Y. Interrogating the Lewis Acidity of Metal Sites in Beta Zeolites with 15N Pyridine Adsorption Coupled with MAS NMR Spectroscopy. *J. Phys. Chem. C* **2016**, *120*, 28533−28544.
(88) Shetty, S.; Kulkarni, B. S.; Kanhere, D. G.; Goursot, A.; Pal, S. A Comparative Study of Structural, Acidic, and Hydrophilic Properties of Sn-BEA with Ti-BEA Using Perioidic Density Functional Theory. *J. Phys. Chem. B* **2008**, *112*, 2573−2579.
(89) Li, G.; Wang, B.; Resasco, D. E. Water-Mediated Heterogeneously Catalyzed Reactions. *ACS Catal.* **2020**, *10*, 1294−1309.
(90) Gould, N. S.; Li, S.; Cho, H. J.; Landfield, H.; Caratzoulas, S.; Vlachos, D.; Bai, P.; Xu, B. Understanding solvent effects on adsorption and protonation in porous catalysts. *Nat. Commun.* **2020**, *11*, No. 1060.
(91) Bregante, D. T.; Tan, J. Z.; Schultz, R. L.; Ayla, E. Z.; Potts, D. S.; Torres, C.; Flaherty, D. W. Catalytic Consequences of Oxidant, Alkene, and Pore Structure on Alkene Epoxidations within Titanium Silicates. *ACS Catal.* **2020**, DOI: 10.1021/acscatal.0c02183.

https://dx.doi.org/10.1021/acs.chemmater.0c02405
Chem. Mater. XXXX, XXX, XXX−XXX